Superconductivity in the three-band model of cuprates: Variational wave function study and relation to the single-band case

M. Zegrodnik,[1,*] A. Biborski,[1,†] M. Fidrysiak,[2,‡] and J. Spałek[2,§]

[1]*Academic Centre for Materials and Nanotechnology, AGH University of Science and Technology, Al. Mickiewicza 30, 30-059 Krakow, Poland*
[2]*Marian Smoluchowski Institute of Physics, Jagiellonian University, ul. Łojasiewicza 11, 30-348 Krakow, Poland*

The d-wave superconductivity (SC) is analyzed within the three-band d-p model with the use of the diagrammatic expansion of the Gutzwiller wave function method (DE-GWF). The determined stability regime of the superconducting state appears in the range of hole doping $\delta \lesssim 0.35$, with the optimal doping close to $\delta \approx 0.19$. The pairing amplitudes between the d orbitals due to copper and p_x/p_y orbitals due to oxygen are analyzed together with the hybrid d-p pairing. The d-d pairing between the nearest-neighboring atomic sites constitutes the dominant contribution to the SC phase. Moreover, it is shown that the decrease of both the Coulomb repulsion on the copper atomic sites (U_d) and the charge-transfer energy between the oxygen and copper atomic sites (ϵ_{dp}) increases the pairing strength as it moves the system from the strong- to the intermediate-correlation regime, where the pairing is maximized. This result is consistent with our analysis of the ratio of changes in the hole content at the d and p orbitals due to doping, which, according to an experimental study, increases with the increasing maximal critical temperature [cf. D. Rybicki *et al.*, Nat. Commun. **7**, 11413 (2016)]. Furthermore, the results for the three-band model are compared to those for the effective single-band picture and similarities between the two approaches are discussed. For the sake of completeness, the normal-state characteristics determined from the DE-GWF approach are compared with those resulting from the variational quantum Monte Carlo method with intersite correlations included through the appropriate Jastrow factors.

I. INTRODUCTION

A complete theoretical description of unconventional superconductivity (SC) in the copper-based materials has long been the subject of debate and still remains an open issue. The main question concerns the microscopic mechanism which can lead to high-temperature superconductivity, as well as the determination of a proper minimal model which would capture its principal properties. Since the cuprates belong to the group of strongly correlated electron systems, the application of standard density functional theory (DFT) *ab initio* calculations seems questionable. On the other hand, methods dedicated specifically to the description of strong electron correlations are involved and their application to significantly simplified models appears as the only feasible approach so far.

It is believed that the copper-oxygen planes, which are common to the whole cuprate family, are instrumental for the formation of the SC phase when the antiferromagnetic charge-transfer insulating parent compound is doped with either electrons or holes [1–3]. Therefore, a significant effort has been devoted to determine which of the copper and oxygen orbitals should be taken into account in the appropriate minimal model. The simplest and most commonly used approach incorporates the copper and oxygen degrees of freedom into

a single-band picture with the Zhang-Rice singlets (ZRSs) [3] playing the role of quasiparticles. In this respect, both Hubbard and t-J models have been intensively investigated [4,5]. Within such an approach the Coulomb repulsion is regarded as the largest parameter in the system that leads to the SC phase due to strong electronic correlations without any explicitly attractive interaction. However, alternative approaches within the weak-coupling scenario, such as the spin-fluctuation-induced pairing, also have been discussed [6], partially in the form adopted for the strong-correlation regime [7]. The strong-correlation-induced SC phase within the t-J model occurs already at the renormalized mean-field theory (RMFT) level [8], whereas for the case of the Hubbard model one has to include the correlation effects beyond the RMFT for the pairing to occur [9–11]. The single-band approach, which combines the features of both t-J and Hubbard models, is the so-called t-J-U model [12–17]. For the latter, we have obtained a very good agreement between theoretical results and the principal experimental observations concerning the pure d-wave SC state [12].

In spite of definite successes of the single-band picture, particular factors influencing the correlation-induced SC state in the Cu-O planes still have not been resolved within that approach. Namely, the doped holes preferentially reside on the oxygen orbitals and a proper partition of the carriers among the Cu and O sites seems to be essential in maximizing the critical temperature T_C [18,19]. In connection to that it has been also argued that the value of the maximal critical temperature is significantly influenced by the value of the charge-transfer gap [20,21], which is determined by the

---

[*]michal.zegrodnik@agh.edu.pl
[†]andrzej.biborski@agh.edu.pl
[‡]maciej.fidrysiak@uj.edu.pl
[§]jozef.spalek@uj.edu.pl

energy distance between the copper and oxygen atomic levels. Under these circumstances an explicit inclusion of the oxygen degrees of freedom should be considered as an important ingredient to be included in any minimal model of hole-doping-induced superconductivity. The simplest model which takes this into account is the three-band model consisting of the $3d_{x^2-y^2}$ orbital due to copper hybridized with $2p_x$ and $2p_y$ orbitals due to oxygen. So far, the application of the dynamical mean-field theory (DMFT) [22,23], variational wave function approach [24], as well as of determinant quantum Monte Carlo [25] methods has led to a reproduction of the charge-transfer insulating phase for the half-filled situation, which corresponds to five valence electrons per $CuO_2{}^{2-}$ complex. Moreover, the appearance of the magnetically ordered [antiferromagnetic (AF)/spin density wave (SDW)] states and superconductivity has been studied with the use of variational wave functions [26–29]. The domelike behavior of the SC amplitude as a function of doping, as well as the anticorrelation between the charge-transfer energy value and the maximal T_C have been reported with the use of the cluster DMFT calculations [20].

Here, we apply the approach based on the Gutzwiller- and Jastrow-type wave functions to study both the selected normal-state characteristics and the paired state within the three-band (d-p) model. The methods in use are as follows: (i) the diagrammatic expansion of the Gutzwiller wave function (DE-GWF) and (ii) the variational quantum Monte Carlo (VMC) with Jastrow correlations. We analyze the pairing amplitudes among the d and p_x/p_y orbitals, as well as the hybrid d-p pairing to determine which states constitute the dominant contribution to the superconducting state. We also show that the Gutzwiller-type variational wave function captures the domelike behavior of the dominant SC amplitude as a function of hole doping. Furthermore, the influence of the charge-transfer energy and the Coulomb repulsion on both the pairing strength and relative occupancy on the d and p orbitals is discussed in the context of experimental observations for the cuprates [19,21]. Throughout our analysis we focus also on comparing the single- and three-band pictures and discuss to what extent the former is efficient in describing the SC phase by relating directly the corresponding macroproperties.

In the following section we present the details of the theoretical model and the applied calculation methods. In Sec. III we first analyze the normal-state characteristics with the use of both VMC and DE-GWF approaches. Next, we move to a detailed analysis of the paired state within the DE-GWF method and compare our results with these for the single-band case. The conclusions are deferred to Sec. IV.

II. MODEL AND METHODS

We start from the three-band d-p model of the form

$$\hat{H} = \sum_{\langle il, jl' \rangle} t_{il}^{ll'} \hat{c}_{il\sigma}^\dagger \hat{c}_{jl'\sigma} + \sum_{il} (\epsilon_l - \mu)\hat{n}_{il} + \sum_{il} U_l \hat{n}_{il\uparrow} \hat{n}_{il\downarrow},$$

$$(1)$$

where $\hat{c}_{il\sigma}^\dagger$ ($\hat{c}_{il\sigma}$) creates (annihilates) the electron with spin σ at the ith atomic site corresponding to an orbital denoted by $l \in \{d, p_x, p_y\}$ and $\langle il, jl' \rangle$ means that the summation is
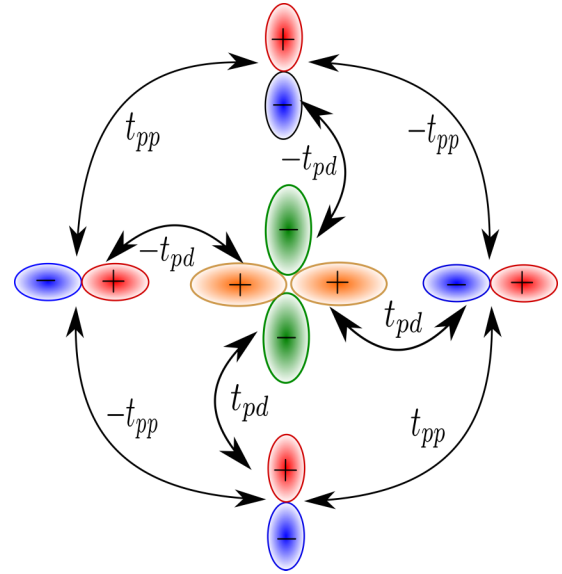
FIG. 1. The hopping parameters between the three types of orbitals in the model and the corresponding sign convention for the antibonding orbital structure. The $d_{x^2-y^2}$ orbital is centered at the copper site and the p_x/p_y orbitals are centered at the oxygen sites.

carried out only for the interorbital nearest-neighbor hoppings (cf. Fig. 1). Note that the p orbitals are located at the oxygen atomic sites which reside in between every two nearest-neighbor copper sites containing the d orbital states (cf. Fig. 1). The wave function phase convention has been taken in the electron representation and is provided in Fig. 1. The second term of the Hamiltonian corresponds to the d and p_x/p_y atomic levels ($\epsilon_{p_x} = \epsilon_{p_y} \equiv \epsilon_p$, $\epsilon_d - \epsilon_p \equiv \epsilon_{dp}$), together with the chemical potential contribution. The interaction parameters U_d and $U_{p_x} = U_{p_y} \equiv U_p$ correspond to the intrasite Coulomb repulsion between two electrons with opposite spins located on the d and p_x/p_y orbitals, respectively.

Hamiltonian (1) expresses an effective description of the Cu-O planes of the copper-based compounds. The values of the hopping and interaction parameters have been evaluated in earlier analyses within the DFT approach [30,31], as well as cluster calculations compared with x-ray photoelectron spectroscopy (XPS) or Auger measurements [32–34]. A more recent analysis with the use of an *ab initio* GW and DFT combination has led to similar values of model parameters obtained within a single scheme [35] which does not suffer from the so-called double counting interaction problem.

The electronic structure corresponding to the single-particle part of Hamiltonian (1), with typical values of the bare hopping parameters $t_{dp} = 1.13$ eV, $t_{pp} = 0.49$ eV, and the charge-transfer energy $\epsilon_{dp} = 3.57$ eV, is shown in Fig. 2 and consists of a hybridized dp antibonding band (red solid line), which crosses the Fermi surface and two fully filled low-energy bands (blue and green solid lines). The typical values of the interaction parameter U_d (U_p) range between 8 and 10.5 eV (4 and 6 eV), depending on the particular approach [30,31,35]. As the value of U_d is significant, the system should be analyzed with the use of a method dedicated to capturing the many-body effects resulting from strong electronic correlations. In our analysis we use two methods, which
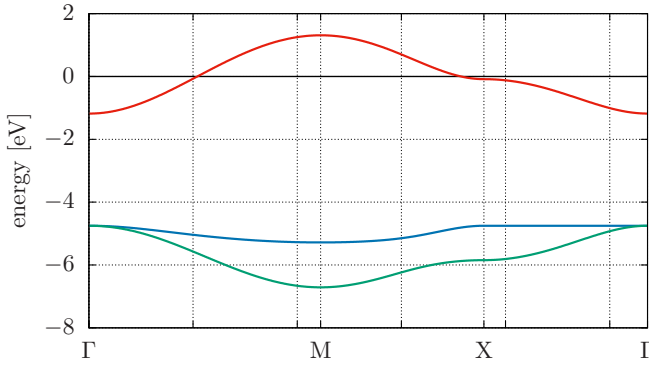
FIG. 2. The electronic structure of the single-particle part of Hamiltonian (1) with parameters $t_{dp} = 1.13$ eV, $t_{pp} = 0.49$ eV, and $\epsilon_{dp} = 3.57$ eV (cf. Fig. 1). The Fermi energy has been taken as the reference value ($E = 0$) on the vertical axis, and corresponds to the case of five electrons per CuO_2 complex, which is referred to as the half-filled situation.

are based on the variational wave functions, namely, the DE-GWF method which allows us to determine the full Gutzwiller wave function solution for an infinite system, and the VMC approach applied for a system of limited size with both the on-site Gutzwiller and intersite Jastrow factors included. To emphasize the effect of strong electronic correlations, the Hartree-Fock results are also provided for comparison.

A. Three-band d-p model within the diagrammatic expansion of the Gutzwiller wave function

A description of the DE-GWF method as applied to the analysis of the SC phase within the single-band t-J, Hubbard, and t-J-U models is provided in Refs. [12,36,37]. The method has been also recently used to study SC in the Anderson lattice model [38] (with reference to the heavy-fermion systems), as well as ferromagnetism and Fermi surface deformations in the two-band Hubbard model [39]. Here, we show some details of the calculation scheme as applied to the three-band d-p model of superconductivity in the cuprates.

The Gutzwiller-type projected many-particle wave function is taken in the form

$$|\Psi_G\rangle \equiv \hat{P}|\Psi_0\rangle = \prod_{il} \hat{P}_{il}|\Psi_0\rangle, \qquad (2)$$

where $|\Psi_0\rangle$ represents the wave function of an uncorrelated SC state. The main difference between the present application and that of the single-band case is that here the situation is orbital dependent, i.e.,

$$\hat{P}_{il} \equiv \sum_\Gamma \lambda_{\Gamma|il}|\Gamma\rangle_{il\ il}\langle\Gamma|, \qquad (3)$$

with $\lambda_{\Gamma|il}$ being the set of variational parameters determining the relative weights corresponding to $|\Gamma\rangle_{il}$, which represent states of the local basis on the atomic sites with the three types of orbitals ($l \in \{d, p_x, p_y\}$),

$$|\Gamma\rangle_{il} \in \{|\varnothing\rangle_{il}, |\uparrow\rangle_{il}, |\downarrow\rangle_{il}, |\uparrow\downarrow\rangle_{il}\}. \qquad (4)$$

The consecutive states represent the empty, singly, and doubly occupied local configurations, respectively. As can be seen,

the variational parameters, which tune the local electronic configurations in the resulting wave function, are orbital dependent.

To simplify significantly the calculations and improve the convergence, one can impose the condition [40,41]

$$\hat{P}_{il}^2 \equiv 1 + x_{il}\hat{d}_{il}^{\text{HF}}, \qquad (5)$$

where x_{il} is yet another variational parameter and $\hat{d}_{il}^{\text{HF}} = \hat{n}_{il\uparrow}^{\text{HF}}\hat{n}_{il\downarrow}^{\text{HF}}$, $\hat{n}_{il\sigma}^{\text{HF}} \equiv \hat{n}_{il\sigma} - n_{l0}$, with $n_{l0} \equiv \langle\Psi_0|\hat{n}_{il\sigma}|\Psi_0\rangle$. By using Eqs. (3) and (5) one can express the parameters $\lambda_{\Gamma|il}$ with the use of x_{il}. Since we are considering a spatially homogeneous state, the i site index in the variational parameters $\lambda_{\Gamma|il}$ and x_{il} can be dropped. Moreover, the oxygen orbitals p_x and p_y are equivalent, which allows us to take $\lambda_{\Gamma|p_x} = \lambda_{\Gamma|p_y} \equiv \lambda_{\Gamma|p}$ and $x_{p_x} = x_{p_y} \equiv x_p$. However, the Coulomb repulsion U_d is different from U_p and the occupancy of the d and p orbitals also, which means that $\lambda_{\Gamma|d} \neq \lambda_{\Gamma|p}$ and $x_d \neq x_p$. In order to simplify further the calculations, one can take $x_p \equiv 0$, for which $\hat{P}_{ip_x} = \hat{P}_{ip_y} = \mathbb{1}$, and then only the copper atomic sites are affected by the correlation operator $\hat{P}$. Such an approximation is justified by the fact that the Coulomb repulsion among the p orbitals is significantly weaker than that corresponding to the d orbitals ($U_d > U_p$). In Appendix A we show that for the parameter regime appropriate for the cuprates such an approximation does not change significantly the obtained results.

In the next step one has to express the expectation values of all the terms appearing in Hamiltonian (1) in the correlated state $|\Psi_G\rangle$. For example, for the hopping term the corresponding expectation value takes the form

$$\langle\Psi_G|\hat{c}_{il\sigma}^\dagger\hat{c}_{jl'\sigma}|\Psi_G\rangle$$
$$= \sum_{k=0}^\infty \frac{1}{k!} {\sum_{m_1 f_1 \dots m_k f_k}}' x_d^{k_d} x_p^{k_p} \langle\tilde{c}_{il\sigma}^\dagger \tilde{c}_{jl\sigma} \hat{d}_{m_1 f_1}^{\text{HF}} \dots \hat{d}_{m_k f_k}^{\text{HF}}\rangle_0, \quad (6)$$

where $\hat{d}_\varnothing^{\text{HF}} \equiv 0$, $\tilde{c}_{il\sigma}^{(\dagger)} \equiv \hat{P}_{il}\hat{c}_{il\sigma}^{(\dagger)}\hat{P}_{il}$, and the index m corresponds to lattice sites, whereas f enumerates the orbitals. The primed summation on the right-hand side is restricted to $(l_h, m_h) \neq (l_{h'}, m_{h'})$, $(l_h, m_h) \neq (i, l)$, and $(l_h, m_h) \neq (j, l')$ for all h, h'. The powers k_d (k_p) express how many times the indices f_h on the right-hand side of Eq. (6) have the value corresponding to the d (p) orbital. For a given k, they fulfill the relation $k_d + k_p = k$. The maximal k, for which the terms in Eq. (6) are taken into account, represents the order of calculations. Similar expressions can be derived for the case of the Coulomb repulsion terms [12]. It has been shown [37,40,42] that the first four to six terms of the expansion lead to a sufficient accuracy of the method. In the subsequent analysis the calculations have been carried out in the third order of the expansion.

Note that the expectation values on the right-hand side of Eq. (6) are taken in the uncorrelated state, $\langle\cdots\rangle_0 \equiv \langle\Psi_0|\cdots|\Psi_0\rangle$, which allows us to carry out the Wicks decomposition in direct space. As a result, one obtains the system energy in the correlated state expressed in terms of the variational parameters x_d, x_p and the uncorrelated expressions of hopping and pairing terms, $P_{ijll''\sigma} \equiv \langle\hat{c}_{il\sigma}^\dagger\hat{c}_{j\sigma}\rangle_0$ and $S_{ijll'} \equiv \langle\hat{c}_{il\uparrow}^\dagger\hat{c}_{jl'\downarrow}^\dagger\rangle_0$, respectively.

To determine explicitly the values of $P_{ijll''\sigma}$ and $S_{ijll''\sigma}$, as well as the variational parameters, the grand canonical

potential $\mathcal{F} = \langle \hat{H} \rangle_G - \mu_G \langle \hat{n} \rangle_G$ is minimized, where $\langle \hat{o} \rangle_G \equiv \langle \Psi_G | \hat{o} | \Psi_G \rangle_G / \langle \Psi_G | \Psi_G \rangle_G$, and μ_G, is the chemical potential. The minimization condition can be cast into the form of a Schrödinger equation with the effective Hamiltonian [36,37]

$$\hat{\mathcal{H}}_{\text{eff}} = \sum_{ijll'\sigma}' t_{ijll'}^{\text{eff}} \hat{c}_{il\sigma}^{\dagger} \hat{c}_{jl'\sigma} + \sum_{il\sigma} \epsilon_{il}^{\text{eff}} \hat{n}_{il\sigma}$$
$$+ \sum_{ijll'} \left(\Delta_{ijll'}^{\text{eff}} \hat{c}_{il\uparrow}^{\dagger} \hat{c}_{jl'\downarrow}^{\dagger} + \text{H.c.} \right), \tag{7}$$

where the primed summation means $i \neq j$ and the effective hopping, effective superconducting gap, and effective atomic level parameters are defined through the relations

$$t_{ijll'}^{\text{eff}} \equiv \frac{\partial \mathcal{F}}{\partial P_{ijll'\sigma}}, \quad \Delta_{ijll'}^{\text{eff}} \equiv \frac{\partial \mathcal{F}}{\partial S_{ijll'}}, \quad \epsilon_{il}^{\text{eff}} \equiv \frac{\partial \mathcal{F}}{\partial n_{il\sigma}^0}. \tag{8}$$

As one can see, the effective Hamiltonian contains both intraorbital ($l = l'$) and interorbital ($l \neq l'$) pairing amplitudes. Nevertheless, all the amplitudes possess d-wave symmetry and no on-site pairing appears. Such a choice is dictated by the experimental findings, according to which the d-wave symmetry of the SC gap is in fact realized in the cuprates [43–46]. The above real-space representation of Eq. (7) can be transformed into reciprocal space and diagonalized through the 6×6 generalized Bogoliubov–de Gennes transformation, on the basis of which the self-consistent equations for the pairing and hopping expectation values can be derived. Within such a scheme, the minimization over the variational parameters x_d and x_p has to be incorporated into the procedure of solving the self-consistent equations.

After all the hopping and pairing lines, together with the variational parameters, are determined, one can calculate next the values of the superconducting pairing amplitudes between particular sites in the correlated state $|\Psi_G\rangle$. In the subsequent section we are going to analyze both the SC pairing amplitudes and the effective gap parameters for the case of intraorbital (d-d, p_x-p_x, and p_y-p_y) and interorbital (d-p_x, d-p_y, and p_x-p_y) pairings between various nearest neighbors in the Cu-O plane. The notation is

$$\Delta_{ll'}^f \equiv \langle \hat{c}_{il\uparrow}^{\dagger} \hat{c}_{jl'\downarrow}^{\dagger} \rangle_G, \quad \Delta_{\text{eff},ll'}^f \equiv \partial \mathcal{F}/\partial S_{ij,ll'}, \tag{9}$$

where the f superscript defines nearest neighbors of a given type. For example, for the case of d-d pairing the SC amplitudes and effective gaps up to the fourth neighbor are determined to be Δ_{dd}^1, Δ_{dd}^3, Δ_{dd}^4, $\Delta_{\text{eff},dd}^1$, $\Delta_{\text{eff},dd}^3$, and $\Delta_{\text{eff},dd}^4$. The second d-d neighbor is excluded, since we are assuming d-wave symmetry. All the correlated pairing amplitudes taken into account in the calculations are marked in Fig. 3. In our notation $\Delta_{p_x p_x}^f$ ($\Delta_{p_y p_y}^f$) corresponds to the p_x-p_x (p_y-p_y) pairing in the (1,0) [(0,1)] direction, whereas $\Delta_{p_x p_x}^{f'}$ ($\Delta_{p_y p_y}^{f'}$) to the p_x-p_x (p_y-p_y) pairing in the (0,1) [(1,0)] direction. The p_x-p_x and p_y-p_y pairing in the (1,0) and (0,1) direction can have different values due to the orientational character of the orbitals. However, the corresponding relation is fulfilled, $\Delta_{p_x p_x}^f = \Delta_{p_y p_y}^{f'}$. This remark applies also to the effective gap parameters which are not marked in Fig. 3 for the sake of clarity.
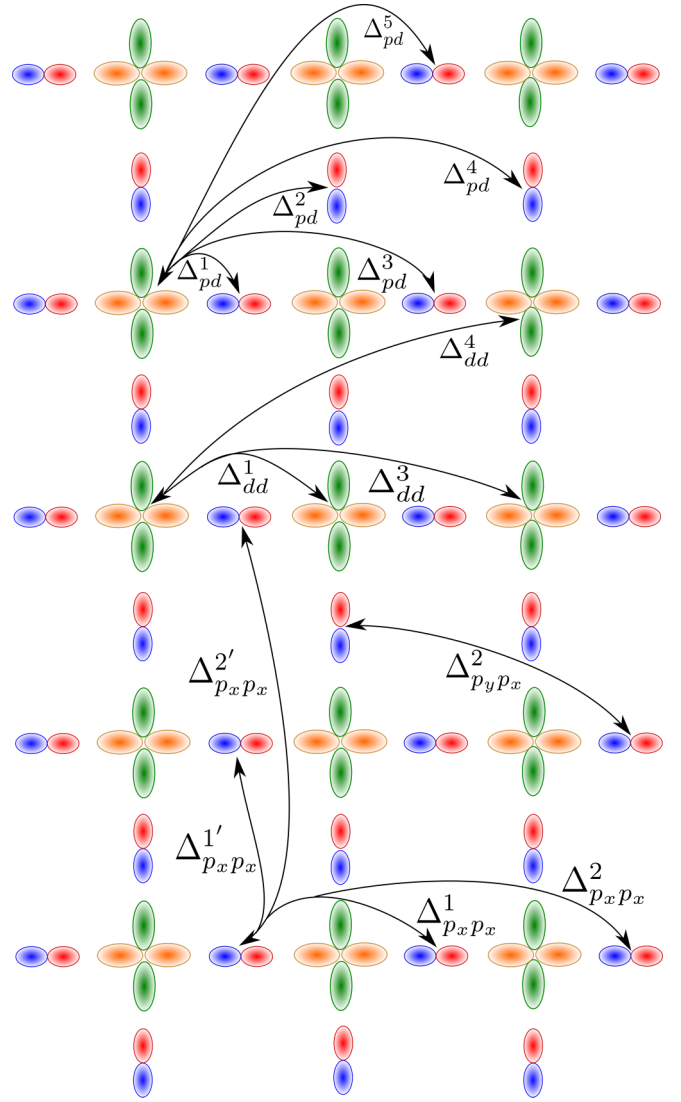
FIG. 3. The component pairing amplitudes in the correlated state $|\Psi_G\rangle$ that are taken into account within our scheme. The superscripts correspond to pairing between consecutive nearest neighbors of a given type (d-d, d-p, p_x-p_x, p_y-p_y, p_y-p_x). The effective gap parameters of corresponding types are also analyzed here, but are not marked for the sake of clarity.

B. Variational Monte Carlo scheme: Application to the three-band d-p model

As a supplementary method which validates the results obtained by means of the DE-GWF formalism for the normal (non-SC) state, we exploit the variational Monte Carlo approach (VMC). The main advantage of VMC relies on the straightforward inclusion of the interelectronic correlations in the wave function optimization scheme. In our situation this is performed in the standard manner, i.e., by using the Jastrow correlation operator $\hat{P}_J$, defined as

$$\hat{P}_J \equiv \exp\left(-\frac{1}{2} \sum_{ij,\mu\nu} \lambda_{ij}^{\mu\nu} \hat{n}_i^{\mu} \hat{n}_j^{\nu} \right), \tag{10}$$
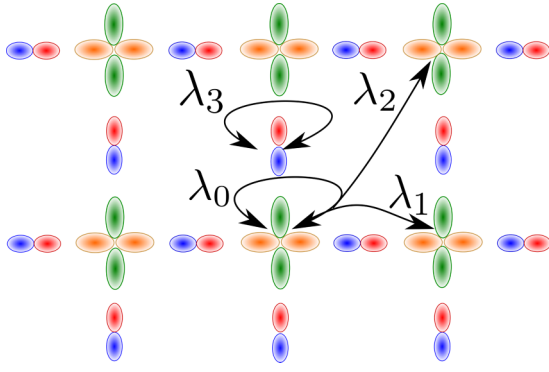
FIG. 4. The Jastrow variational parameters considered in the VMC analysis. Site-orbital indices are labeled as indicated.

where $\hat{P}_J$ with μ, $\nu \in \{d, p_x, p_y\}$ acts as before on the uncorrelated state $|\Psi_0\rangle$, and $\{\lambda_{ij}^{\mu\nu}\}$ are the variational parameters, which are optimized via the VMC scheme. The details of the VMC procedure may be found in Refs. [47,48]. Here, we have employed the self-developed code [49], which has been recently applied in the variance optimization scheme for the analysis of the molecular hydrogen metallization [50]. In this study, the *energy optimization* is carried out, since it is considered to be more robust in conjunction with the *stochastic reconfiguration* (SR) [47] technique. As VMC operates in real space, the considered systems are *finite* clusters. To minimize the influence of the size factor, we have imposed periodic boundary conditions (PBCs) in our calculations. We have selected variational parameters to obtain the essential properties of the normal state. Moreover, we found out that the inclusion of particular types of parameters affects the numerical stability of the whole optimization procedure. This is the case with the nearest-neighbor d-p variational parameter λ_{ij}^{dp}. Eventually, after a number of testing simulations we decided to limit ourselves to the parameters presented in Fig. 4 (note that we provided the relabeling of the Jastrow variational parameters for the sake of brevity). We find this selection as a compromise between reliability (i.e., trial wave function flexibility) and numerical stability.

III. RESULTS AND DISCUSSION

In this section we study both the principal normal-state characteristics and d-wave superconductivity for the case of the three-band d-p model with either electron or hole doping. In all the figures the zero doping ($\delta = 0$) case corresponds to the parent compound for which each CuO$_2$ complex is occupied by five electrons ($n_{tot} = 5$). Such a situation is going to be referred to as that of half filling. The $\delta > 0$ ($\delta < 0$) situation refers to the hole (electron) doping with $n_{tot} < 5$ ($n_{tot} > 5$). If not stated otherwise, we set the hopping parameters and charge-transfer energy to $t_{dp} = 1.13$ eV, $t_{pp} = 0.49$ eV, and $\epsilon_{dp} = 3.57$ eV. The interaction parameters U_d and U_p are specified explicitly in each analyzed case.

A. Normal-state characteristics

In Figs. 5 and 6 we show the orbital-resolved double occupancies $d_d^2 = \langle \hat{n}_{id\uparrow} \hat{n}_{id\downarrow} \rangle_G$ and $d_p^2 = \langle \hat{n}_{ip_x\uparrow} \hat{n}_{ip_x\downarrow} \rangle_G =$
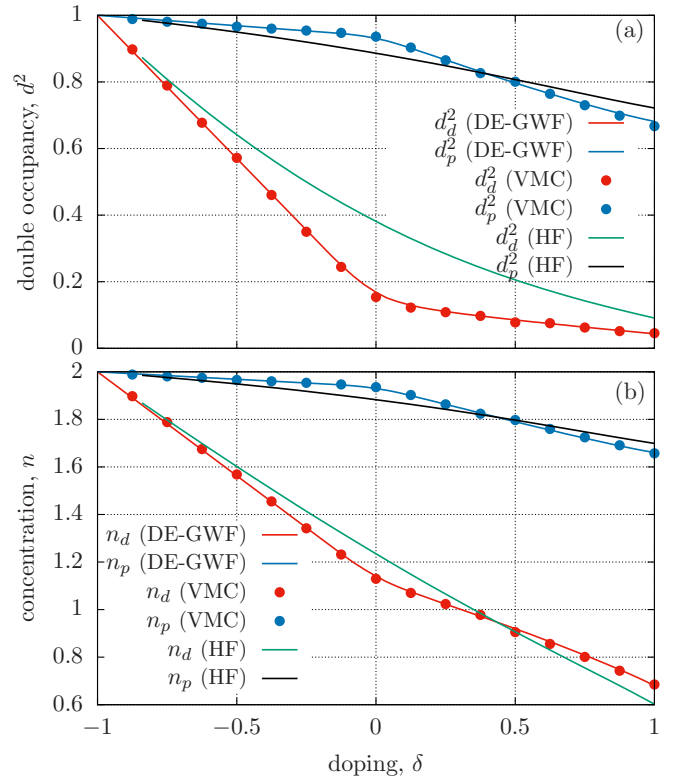
FIG. 5. (a) Orbital-resolved double occupancies and (b) component electron concentrations as a function of doping for $U_d = 7.85$ eV and $U_p = 4.1$ eV, for three different methods: DE-GWF, VMC, and HF. For $\delta > 0$ ($\delta < 0$) we have the hole- (electron-) doped case with $n_{tot} < 5$ ($n_{tot} > 5$).

$\langle \hat{n}_{ip_y\uparrow} \hat{n}_{ip_y\downarrow} \rangle_G$, electron concentrations n_d and n_p, as well as the ground-state energy, all as a function of doping. For comparison, the calculations have been carried out by the DE-GWF and VMC methods which take into account the correlation effects, as well as the Hartree-Fock (HF) approximation which disregards them. It should be noted that the VMC method includes both intra- and interside correlation operators for system sizes of 4×4 CuO$_2$ complexes, whereas within the DE-GWF approach we carry out calculations for an infinite system. However, for the latter approach only the on-site
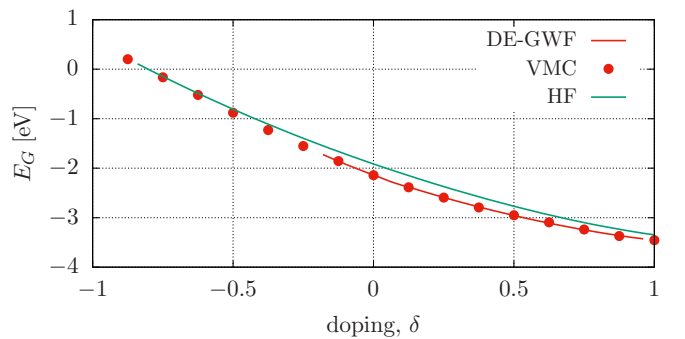
FIG. 6. Ground-state energy as a function of doping for $U_d = 7.85$ eV and $U_p = 4.1$ eV for three different methods: DE-GWF, VMC, and HF. For $\delta > 0$ ($\delta < 0$) we have the hole- (electron-) doped case with $n_{tot} < 5$ ($n_{tot} > 5$).

Gutzwiller operator for the copper atomic sites is introduced (cf. Sec. II). As one can see, in spite of the formal differences, both methods provide very similar results with a characteristic kink in both the double occupancies and electron concentration that appears at half filling. Within the Hartree-Fock approach such a kink is absent and a smooth behavior is observed when passing through the $\delta = 0$ point, indicating that the kinks result from the correlations. Obviously, HF calculations lead to a visibly higher system energy than that in the DE-GWF and VMC methods (cf. Fig. 6). As one can see, in the hole-doped range ($\delta > 0$) we have $n_d \lesssim 1$ and, due to the high value of U_d, the double occupancies at d orbitals are kept relatively small and weakly dependent on the doping. As we increase the number of particles above $n_{tot} = 5$ (electron doping, $\delta < 0$), the oxygen orbitals are almost completely full, $n_p \approx 2$ with $d_p^2 \approx 1$, and the remaining electrons are forced to occupy the copper orbitals, resulting in a visible change of slope in d_d^2 and n_d. A similar effect, obtained here by the use of variational wave functions, has also been reported within the determinant quantum Monte Carlo approach [25], as well as in DMFT calculations [22].

It has been argued in Ref. [19] that the ratio of respective changes in the hole content on the d and p orbitals ($\rho = \Delta \tilde{n}_d / 2\Delta \tilde{n}_p$, where $\tilde{n}_d = 2 - n_d$, $\tilde{n}_p = 2 - n_p$), as one increases the number of carriers, is a family property (cf. Fig. 2 in Ref. [19]). Moreover, it appears that for the case of hole-doped compounds the smaller ρ is, the smaller is the maximal critical temperature of a given group of compounds. In Fig. 7 we draw the $\tilde{n}_d$ vs $\tilde{n}_p$ plot which illustrates the local charge distribution on the $(\tilde{n}_d, 2\tilde{n}_p)$ plane. The parameter ρ within either the hole- or electron-doping regime can be extracted from the slope of the $\tilde{n}_d(2\tilde{n}_p)$ dependence and the horizontal axis. The yellow solid line in the figure represents the parent compound (one hole per CuO_2 complex when $\tilde{n}_d + 2\tilde{n}_p = 1$), the upper-right half of the $(2\tilde{n}_p, \tilde{n}_d)$ plane corresponds to hole doping, and the lower-left to electron doping. As one can see, by comparing the DE-GWF/VMC results with those corresponding from the HF approach, the value of ρ in the hole-doped regime is significantly suppressed by the correlation effects taken into account by the variational wave functions. Namely, for DE-GWF/VMC we obtain $\rho \approx 0.72$, while for HF the result is $\rho \approx 2.0$. The experimental values are in the regime $\rho < 1$ [19], reaching even 0.2 for La-214. We conclude that the low values of ρ for the hole-doped cuprates are a signature of strong electron correlations.

In Fig. 7(b) we show the $\tilde{n}_d(2\tilde{n}_p)$ dependence in the hole-doped region for different values of the model parameters according to DE-GWF (solid line) and VMC (circles). For each set of parameters the approximate value of ρ is determined by fitting the linear plot to our VMC results. As one can see, a reduction of ϵ_{dp} by 2 eV, with all other parameters fixed, does not lead to any significant increase of ρ (black and green data set). Nevertheless, the plot is shifted towards lower $\tilde{n}_d$ and higher $\tilde{n}_p$ values. A similar result, but with an additional increase of the ρ parameter, is obtained by lowering the U_d value (violet, black, and blue data sets). As shown experimentally, both of these effects are related to an enhancement of the critical temperature in the cuprates [19]. Obviously, in a realistic situation, U_d and ϵ_{dp} vary between different compounds. According to the recent *ab initio* cal-
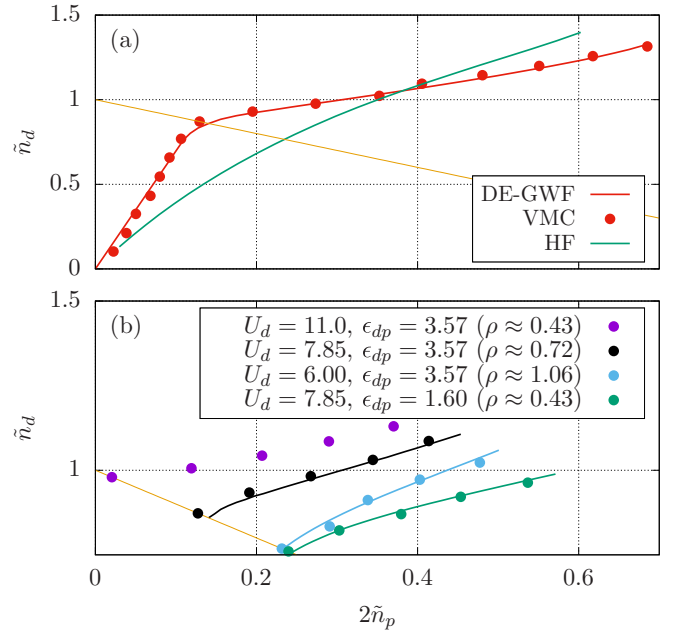
FIG. 7. (a) Hole content distribution in the $(\tilde{n}_d, 2\tilde{n}_p)$ plane calculated according to the DE-GWF, VMC, and HF methods for $U_d = 7.85$ and $U_p = 4.1$ eV. Different points of the plots refer to different values of doping (δ). The solid dark blue line corresponds to the parent compound $\delta = 0$, and the upper-right (lower-left) half of the plane refers to the hole-doped (electron-doped) case. (b) Hole content distribution between the d and p orbitals for different sets of model parameters for the hole-doped situation within the DE-GWF (solid lines) and VMC (circles) methods. For each set the charge distribution ratio, $\rho = \Delta \tilde{n}_d / 2\Delta \tilde{n}_p$, has been determined by fitting a linear plot to the VMC data.

culations [35] for the two systems with significantly different maximal critical temperatures ($HgBa_2CuO_4$ with $T_C \approx 90$ K and La_2CuO_4 with $T_C \approx 40$ K), both the lower U_d and ϵ_{dp} values correspond to the compound with a higher maximal T_C. This issue is discussed further below, where the paired phase is analyzed in detail.

B. Superconducting gaps in the three-band model and their single-band correspondent

In this section we focus on the analysis of a paired state within the three-band model for the case of hole doping ($\delta > 0$) within the DE-GWF method. In Figs. 8(a), 8(c) and 8(d) we show the doping dependences of the intra- and interorbital pairing amplitudes in the correlated state [cf. Fig. 3 and Eq. (9)]. As one can see, the dominant contribution to the superconducting state results from the pairing between the d orbitals residing on the nearest-neighbor copper atomic sites [Δ_{dd}^1 in Fig. 8(a)]. The $\Delta_{dd}^1(\delta)$ function reproduces the domelike behavior with the maximum value corresponding to the optimal doping, $\delta \approx 0.19$. The maximal values of all the other pairing amplitudes in Figs. 8(a), 8(c) and 8(d) represent at most 20% of that corresponding to Δ_{dd}^1. Note that even though the nearest-neighbor mixed d-p (Δ_{dp}^1) amplitude corresponds to pairing between atomic sites which are twice as close to each other as for the case of Δ_{dd}^1, the latter plays the
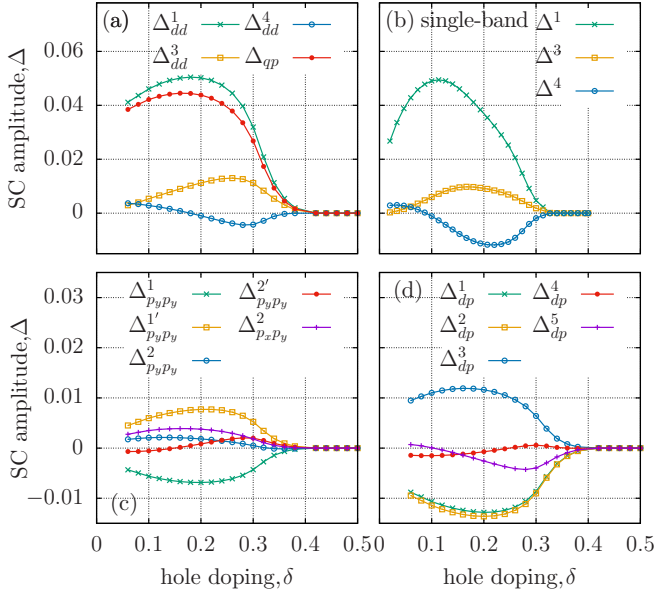
FIG. 8. Pairing amplitudes between (a) d-d, (c) p-p, and (d) d-p atomic sites as a function of doping for $U_d = 10.3$ eV, $U_p = 4.1$ eV [cf. Fig. 3 and Eq. (9)]. Additionally, in (a) we show the quasiparticle gap amplitude (Δ_{qp}) which is defined in the main text. In (b) we show the first-, third-, and fourth-nearest-neighbor pairing amplitudes for the case of a single-band Hubbard model with $t = -0.35$ eV, $t' = 0.25|t|$, and $U = 6$ eV.

most important role. It is due to the fact that large U_d generates the electron correlations which in turn lead to the paired state. Therefore, the nearest-neighbor sites with the largest Coulomb repulsion constitute the dominant contribution.

For the sake of comparison, in Fig. 8(b), we show the analogous results for the case of a single-band Hubbard model on a square lattice with typical values of the model parameters corresponding to the cuprates, $t = -0.35$ eV, $t' = 0.25|t|$, and $U = 6$ eV, which refer to the nearest- and next-nearest-neighbor hopping and the on-site Coulomb repulsion, respectively. We plot the SC amplitudes for the first-, third-, and fourth-nearest neighbors (second is zero due to the d-wave symmetry of the SC state). Note that the doping dependences of the SC amplitudes are quite similar to those corresponding to the d orbitals in the three-band case [cf. Figs. 8(a) and 8(b)]. These two figures speak to the validity of the single-band picture as far as the SC amplitudes are concerned.

Additionally, in the three-band case we calculate the SC amplitude $\Delta_{\mathrm{qp}} = \langle \hat{\alpha}_{i\uparrow}^{\dagger} \hat{\alpha}_{j\downarrow}^{\dagger} \rangle_G$ [Fig. 8(a)], where $\hat{\alpha}_{i\sigma}^{\dagger}$ are the quasiparticle operators for the hybridized antibonding band which crosses the Fermi surface in the normal state (red solid line in Fig. 2). This is the most representative pairing amplitude in the three-band model since the SC gap is formed around the Fermi surface and the mentioned hybridized band becomes gapped in the SC phase. Since Δ_{dd}^1 has the dominant contribution to the paired state, the behavior of Δ_{qp} is mostly determined by the former, as can be clearly seen in Fig. 8(a).

In the three-band case, we have not obtained convergence close to the half-filled situation for $U_d = 10.3$ eV. This is the reason why the plots in Fig. 8 are drawn only down to $\delta \approx 0.06$. It is not clear if the SC pairing amplitudes drop to zero,
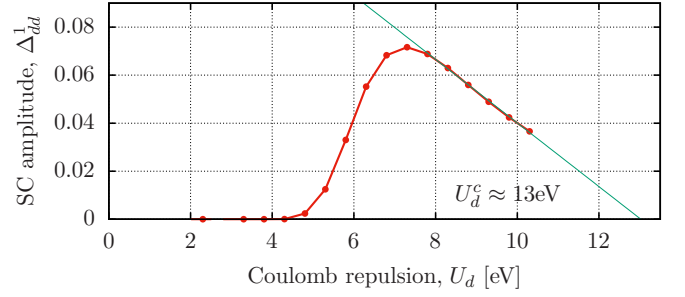
FIG. 9. The nearest-neighbor d-d pairing amplitude for the case of half filling, $\delta = 0$, as a function of U_d for $U_p = 4.1$ eV. For $U_d \gtrsim 10$ eV the convergence could not be reached and the critical value of U_d for which Δ_{dd} is suppressed is evaluated by carrying out a linear extrapolation which leads to the critical value $U_d^c \approx 13$ eV.

as we reach the half-filled situation. In Fig. 9 we show the dominant Δ_{dd}^1 amplitude for $\delta = 0$ as a function of U_d up to the highest value of U_d for which the convergence could be obtained. By carrying out a linear extrapolation to the high-U_d region we estimate that the SC amplitude is completely suppressed above the upper critical value $U_d = U_d^c \approx 13$ eV.

In Fig. 10 we display the effective SC gaps as a function of doping, both for the three-band [Figs. 10(a) and 10(b)] and single-band cases [Fig. 10(c)] for the same values of model parameters as those selected in Fig. 8. As one could expect, also here the dominant contribution comes from the nearest-neighbor d-d pairing. However, in contrast to the pairing amplitudes shown in Fig. 8, the dominant effective
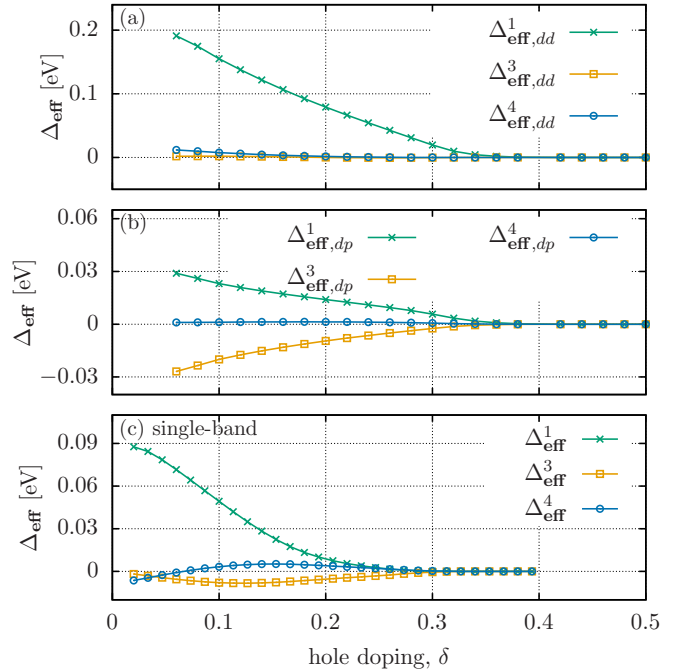
FIG. 10. Effective superconducting gaps between (a) d-d and (b) d-p orbitals as a function of doping for $U_d = 10.3$ eV, $U_p = 4.1$ eV [cf. Fig. 3 and Eq. (9)]. The calculated p-p effective gaps are zero. In (c) we show the first-, third-, and fourth-nearest-neighbor effective gaps for the case of a single-band Hubbard model with $t = -0.35$ eV, $t' = 0.25|t|$, and $U = 6$ eV.
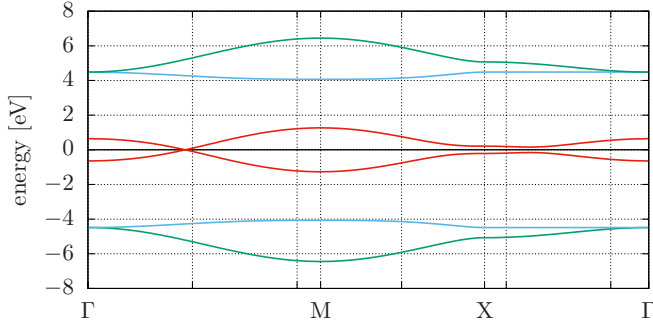
FIG. 11. Quasiparticle dispersion relations in the SC state for $\delta = 0.24$ and for the same model parameters as in Figs. 8 and 10.

gap increases as one approaches the half-filled situation. Such a behavior has also been reported for the case of a single-band Hubbard model analyzed within the VMC approach [9] and for the DE-GWF calculations for the single-band t-J [37] and t-J-U [14] models. It should be noted that the effective SC gaps within the p-orbital sector are zero even though the corresponding pairing correlations have nonzero values [cf. Figs. 8(c) and 8(d)]. This is because electrons residing on p orbitals are not significantly correlated due to the small value of U_p in comparison to U_d. Therefore, the pairing correlations between the p orbitals are induced by the appearance of both d-d and d-p pairings, in a manner analogous to the proximity effect in superconductor–normal-metal heterostructures. However, such induced p-p pairing correlations do not contribute to the spectral gap, meaning that $\Delta_{\mathrm{eff},pp} \equiv 0$. The quasiparticle dispersion relations which result from the effective Hamiltonian (7) for the SC phase and for selected values of doping ($\delta = 0.24$) are shown in Fig. 11. As one can see, the antibonding hybridized band (red solid line) is gapped apart from the nodal point between Γ and M due to the d-wave symmetry of the SC gap. A similar band structure appears for other dopings. This quasiparticle structure can be compared with that for bare bands in the normal state, which is depicted in Fig. 2.

C. Overall behavior and phase diagram

Next, we turn to the analysis of the question how the values of the U_d and ϵ_{dp} parameters influence the details of the SC state. In Fig. 12 we show the maps of quasiparticle pairing amplitude in (U_d, δ) space for two selected values of ϵ_{dp} which differ by 2 eV. Both of them can be regarded as realistic for selected cuprates. Again, the maps resemble those for the single-band Hubbard or t-J-U models (cf. Figs. 3 and 4 in Ref. [12]), with the paired phase appearing for high enough values of the Coulomb interaction and confined to the region with $\delta \lesssim 0.35$.

Also, in both single- and three-band cases one can single out three distinct regions: (i) a weak-correlation regime (low U or U_d) for which the pairing amplitude increases with increasing U or U_d; (ii) the intermediate-correlation regime placed around the maximum of the pairing amplitude as a function of U or U_d; and (iii) the strong-correlation regime, with large U or U_d in which the pairing amplitude is decreasing back with increasing U or U_d. In the single-band approach
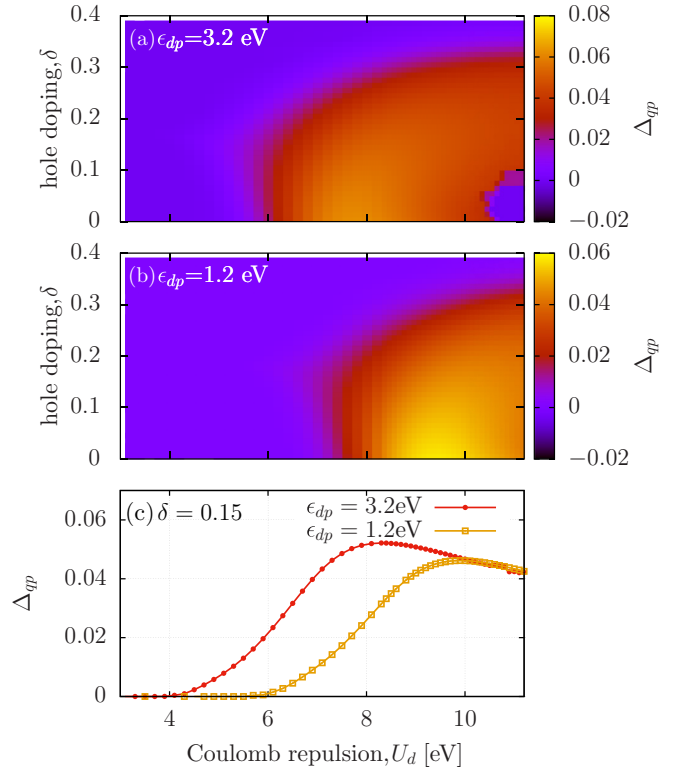
FIG. 12. The quasiparticle superconducting gap Δ_{qp} as a function of doping and Coulomb repulsion on the d orbitals for (a) $\epsilon_{dp} = 3.2$ eV and (b) $\epsilon_{dp} = 1.2$ eV; $U_p = 4.1$ eV. (c) $\Delta_{\mathrm{qp}}(U_d)$ plots for $\delta = 0.15$ and for the two values of ϵ_{dp}, as for (a) and (b). The irregular region with $\Delta_{\mathrm{qp}} = 0$ for high values of U_d close to $\delta = 0$ in (a) is where we could not achieve convergence within our computational scheme.

the intermediate-correlation regime appears close to $U \approx W$, where W is the bare bandwidth. It is not clear what parameter determines the corresponding critical value of U_d in the three-band case. From our analysis we can see that in the three-band model the sequence of the three regimes may be shifted on the U_d axis by changing ϵ_{dp}, which does not have its analog in the single-band case. In Fig. 12(c) we illustrate that effect by drawing Δ_{qp} vs δ for two values of ϵ_{dp}, which differ by 2 eV. As one can see, the maximal value of Δ_{qp} as a function of U_d is shifted also by about 2 eV. However, the corresponding change of the hybridized antibonding bandwidth is only ≈ 1 eV. Such a situation can be understood by looking at the energy change corresponding to the electron transfer from the oxygen atomic site to the nearest-neighbor copper atomic site for the parent compound. It is equal to $\Delta E = U_d - U_p + \epsilon_{dp}$ and corresponds to the lowest-energy excitation. The value of ΔE should be considered as that determining the strength of the electron correlations. By reducing ϵ_{dp} by 2 eV one also reduces ΔE, therefore the strong-correlation regime moves by 2 eV towards higher U_d values, which is actually seen in Fig. 12.

Since the high-temperature superconductors are placed in the strong-correlation regime, but close to the intermediate one, the decrease of both U_d and ϵ_{dp} results in a shift towards the intermediate regime, where the higher values of the pairing
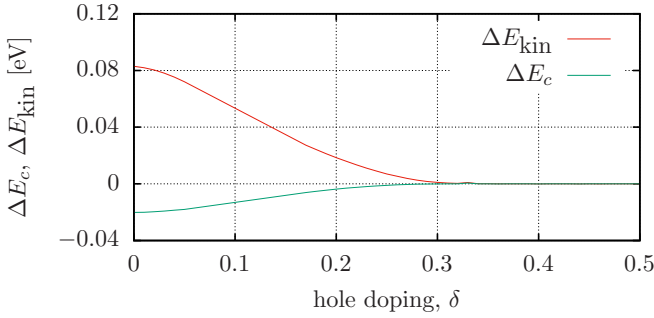
FIG. 13. Superconducting condensation energy and kinetic energy gain at the transition to the SC phase as a function of doping for $\epsilon_{dp} = 3.2$ eV and $U = 7.9$ eV.

amplitudes appear. Such a conclusion is in agreement with our analysis of the hole content distribution [$\tilde{n}_d(2\tilde{n}_p)$], according to which for lower values of U_d and ϵ_{dp} the ρ parameter increases together with the decrease of copper-hole content, in favor of the oxygen-hole content for the parent compound. It has been reported experimentally that such changes correspond to an enhancement of the maximal value of T_C [19].

We have encountered technical problems with the convergence of our computational scheme for the electron-doped regime $\delta < 0$. At present, we are able to calculate only a small part of that side of the phase diagram. Such incomplete results are not shown here. In general, one expects that the SC state should be less pronounced for $\delta < 0$, as seen in experiment [51] and reproduced within the single-band approach [14]. Note that for the case of electron doping the oxygen atomic sites are practically fully occupied, as seen in Fig. 5 ($n_p \approx 2$ and $d_p^2 \approx 1$). Therefore, the doped electrons go mainly into the copper d orbitals and the oxygen degrees of freedom are frozen. In such a situation, the electron-hole asymmetry obtained within the single-band case is expected to be approximately correct in the d-p model.

For the sake of completeness, in Fig. 13 we plot the superconducting condensation energy (ΔE_c) and the kinetic energy change at the SC transition (ΔE_{kin}). The latter is defined in the following manner,

$$\Delta E_{kin} \equiv E_{G|0}^{SC} - E_{G|0}^{PM}, \quad E_{G|0} \equiv \frac{1}{N} \sum_{ij\sigma}' t_{ij} \langle \hat{c}_{i\sigma}^\dagger \hat{c}_{j\sigma} \rangle_G, \quad (11)$$

where the kinetic energy difference is taken between the superconducting (SC) and normal paramagnetic (PM) states. The condensation energy, corresponding to the total ground-state-energy difference, $\Delta E_c \equiv E_G^{SC} - E_G^{PM}$, should be negative for the SC phase to be stable, which is indeed the case (cf. green solid line in Fig. 13). However, the values of ΔE_{kin} are positive (red solid line in Fig. 13), which means that the transition to the SC state is driven by the Coulomb interaction energy. Positive values of ΔE_{kin} are also known from the BCS theory of conventional superconductors. The same situation takes place in the single-band Hubbard model for $U \lesssim W$ [12]. However, in the latter model also negative values of ΔE_{kin} are reported (non-BCS behavior) in the wide doping range after increasing the U parameter [cf. Fig. 3(a) in Ref. [12]]. Unfortunately, for the three-band-model case, we have encountered problems with convergence for large U_d

values. Therefore, we have not been able to verify if also in the present case the negative values of ΔE_{kin} can appear for large enough U_d. Note that it has been reported experimentally that in the cuprates the transition between positive and negative values of ΔE_{kin} appears close to the optimal doping [12], with $\Delta E_{kin} < 0$ for the underdoped samples. This feature, which neither appears here nor for the single-band Hubbard model case, can be reproduced very well within the so-called t-J-U model [12]. In this context, it is worth mentioning that a natural extension of the t-J-U model to the three-band situation would involve inclusion of both the intersite Kondo (d-p) and kinetic (d-d) exchange interactions. Such a model would comprise explicitly the dynamic intersite correlations into our Gutzwiller-type wave function with intrasite projections only. Then, the starting model would take the form of a mixed three-band+Emery-Reiter model [4].

IV. CONCLUSIONS AND OUTLOOK

By analyzing the normal-state characteristics we have shown that the correlation effects taken into account by either a Gutzwiller- or Jastrow-type variational wave function lead to kinks in the orbitally resolved double occupancy and electron concentration for half filling in the three-band d-p model (cf. Fig. 5), which have also been reported by other methods [22,25] dedicated to strongly correlated systems, and do not appear in the Hartree-Fock approximation. In this respect, the correlations alter significantly the role of the ρ parameter, reducing it in the hole-doped regime and increasing its value for the case of electron doping (cf. Fig. 7). Therefore, the low values of ρ measured in the hole-doped cuprates with the lowest experimentally determined $\rho \approx 0.2$ (for La-214) [19] should be considered as a signature of strong electron correlations. The values of ρ obtained here ($\rho \approx 0.7$-1.0) within DE-GWF/VMC calculations correspond to those observed for Bi-, Hg-, and Tl-based cuprate compounds [19].

We have analyzed the paired phase in the three-band d-p model with the use of the DE-GWF method and have shown that due to the electron correlation effects, the SC state is stable in the doping region $\delta \lesssim 0.35$, with the maximal value of the dominant d-d pairing amplitude appearing at $\delta \approx 0.19$ (optimal doping). Those values correspond well with those determined in the single-band calculations [12,37] and in numerous experimental situations for the cuprates [2].

Within the three-band model the dominant contribution to the SC state emerges from the pairing between the nearest-neighbor d-d atomic sites, which also reflects primarily the behavior of the quasiparticle gap in the antibonding hybridized band. The calculated pairing amplitudes between the copper atomic sites trace the corresponding nearest-neighbor gaps for the square lattice treated within the single-band Hubbard model [cf. Figs. 8(a) and 8(b)]. Such a connection is also reproduced for the calculated effective gaps [cf. Figs. 10(a) and 10(c)]. Another similarity between the single- and three-band models is the characteristic behavior of the pairing amplitude as a function of both δ and U_d (U for the single-band case), with the weakly, intermediate, and strongly correlated regimes visible (cf. Fig. 12 here and Figs. 3 and 4 in Ref. [12]). Note that the close relation between the relevant subbands of the three- and single-band models has

been reported in Ref. [52] with the use of a composite operator method. However, that analysis did not include the paired states. On the other hand, the differences between the single- and three-band pictures of the cuprates with respect to the strength of spin fluctuations, as well as their relation to the pairing mechanism, have been singled out in Refs. [53,54].

In spite of the mentioned similarities there are some aspects of high-T_C cuprates that cannot be analyzed within the single-band approach. Namely, the charge-transfer energy (ϵ_{dp}), which does not possess its correspondent in the single-band case, tunes the strength of the correlations. For smaller ϵ_{dp} values the correlations seem to be suppressed, which means that a stronger Coulomb repulsion (U_d) is necessary to induce the SC state. Also, since the copper-based materials are placed in the strongly correlated regime close to the intermediate one, it results from our analysis that by decreasing ϵ_{dp} and U_d one moves towards the intermediate-correlation regime, where the values of the pairing amplitudes are higher. This in turn may lead to a higher critical temperature. Such a conclusion is in agreement with our analysis of the hole content distribution and the experimental findings, according to which the reduction of the hole content at copper sites in favor of oxygen sites in both the parent compound and hole-doped situation leads to an enhancement of the maximal critical temperature [19]. At the present stage of our research the agreement with the mentioned experiments is only qualitative, since we have not been able to fit directly to the measured copper and oxygen hole contents and obtain the changes of the pairing amplitudes, which would correspond to the reported T_C for different cuprate compounds (cf. Fig. 2 in Ref. [19]). For example, the experiments for La-214 report $\rho \sim 0.2$, and such low values cannot be reproduced in our theoretical approach within the range of realistic model parameters. The fact that there is a correlation between the apical oxygen distance and the value of ρ suggests that to achieve a quantitative agreement between theory and experiment, one should include those apical oxygen states in a manner presented in Ref. [55].

According to experimental observations, the AF phase appears in the cuprate family for very low hole doping, i.e., below $\delta_c^{AF} \approx 0.05$ [56]. Such a value has been reproduced by some of the theoretical investigations within both the single- and three-band pictures [11,20,57]. As we show in Appendix B, the dominant spin-spin correlation, which corresponds to the $\mathbf{Q} = (\pi, \pi)$ ordering vector, is reproduced within our approach for $\delta = 0$. Due to small experimental critical doping δ_c^{AF}, the region in which a possible interplay between SC and AF appears should not be significant in comparison with the SC stability range (up to $\delta \approx 0.3$–0.4). Therefore, since we are mainly focused on the paired phase characteristics, we did not include the AF and SC orderings simultaneously in our analysis. As we have shown here, the dominant contribution to the pairing comes from the nearest-neighbor d orbitals, the same orbitals on which a staggered magnetic structure is formed in the AF state. As a consequence, the presented results, which correspond to the SC state, should be modified by the appearance of the AF ordering in the region close to half filling. In particular, as shown in the single-band picture, it may induce a minor spin-triplet component to the pairing [11,42,58]. When it comes to the three-band calculations some of the analysis did not report

a significant coexistence region [20]. On the other hand, the AF+SC phase appeared as stable in other reports, for which the δ_c^{AF} value turned out to be larger than the experimental one [29]. This issue requires a separate analysis.

At the end, it should be noted that the VMC calculations have been carried out for limited systems consisting of 4×4 CuO$_2$ complexes, whereas the DE-GWF method allows for an analysis of infinite systems. Also, within the DE-GWF approach, we included only an on-site correlation operator acting on the copper atomic sites, whereas within the VMC calculations a more involved wave function has been applied with the intersite Jastrow factors. In spite of those differences, the agreement between the two methods is very good (cf. Figs. 5 and 7). This last feature speaks again for the dominant role of the Cu d electrons.

APPENDIX A

Here, we show that in a parameter regime significant for the cuprates it is justified to apply the approximation for which $x_p \equiv 0$. In such a situation the correlation operator from Eq. (3) acts only on the copper atomic sites, which simplifies significantly the calculations. Nevertheless, the electron correlations, which result from the dominant interaction (U_d) in the system, are taken into account by minimizing the system energy over x_d. In Fig. 14 we show the double occupancies
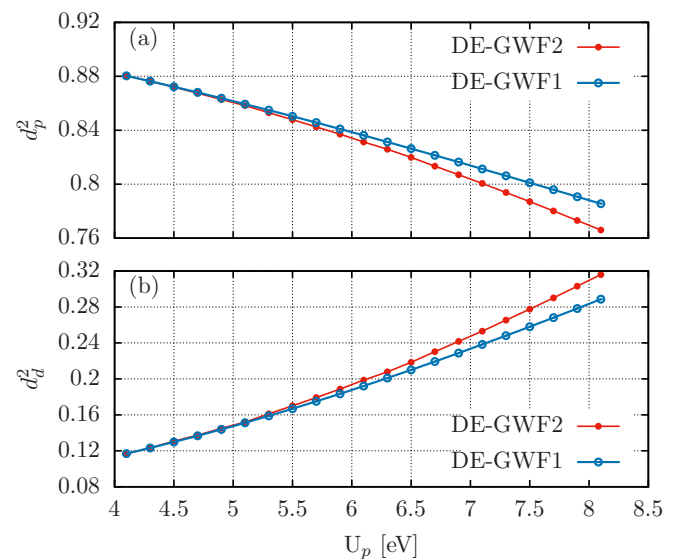
FIG. 14. Double occupancies on the (a) oxygen and (b) copper atomic sites as a function of U_p for $U_d = 7.85$ eV and $\delta = 0.2$ calculated by two variants of the DE-GWF scheme. In the first one (DE-GWF1) we fix $x_p \equiv 0$ and minimize only over x_d, whereas in the second (DE-GWF2) the full minimization over both x_d and x_p is carried out.
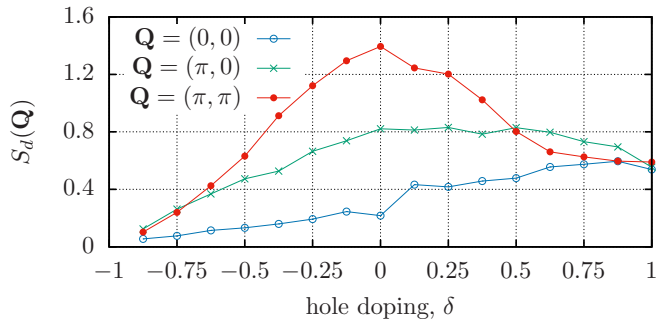
FIG. 15. The spin-spin correlation function between the copper orbitals as a function of doping for three selected ordering vectors. The calculations have been obtained within the VMC approach for the system containing 4×4 CuO_2 complexes.

on the copper and oxygen atomic sites as a function of U_p calculated within the DE-GWF method by assuming either $x_p \equiv 0$ (DE-GWF1), or obtained by using the complete form of the correlation operator (3), i.e., minimization over both x_d and x_p (DE-GWF2). As one can see, the differences between the two calculation schemes become visible as one increases

the value of U_p. Nevertheless, for $U_p \approx 4$–6 eV, appropriate for the cuprates, the results practically coincide.

APPENDIX B

In this Appendix we present the spin-spin correlation function at the copper d orbitals for three selected ordering vectors. The correlation function is defined as follows,

$$S_d(\mathbf{Q}) = \frac{1}{N} \sum_{ij} e^{i\mathbf{Q} \cdot \Delta \mathbf{R}_{ij}} \langle \hat{m}_{id} \hat{m}_{jd} \rangle, \quad \text{(B1)}$$

where $\Delta \mathbf{R}_{ij} = \mathbf{R}_i - \mathbf{R}_j$ is the vector connecting two Cu lattice sites and $\hat{m}_{id} = \hat{n}_{id\uparrow} - \hat{n}_{id\downarrow}$ is the magnetization on the ith Cu lattice site. As one can see from Fig. 15, there is a dominant tendency towards antiferromagnetic ordering with $\mathbf{Q} = (\pi, \pi)$ at half filling, which is being suppressed with increasing hole doping. Unfortunately, by looking at the correlation functions we are not able to determine the upper critical doping for the appearance of the AF order in the system. Nevertheless, this result is in qualitative agreement with the one presented in Ref. [25] (Fig. 9), where the calculations have been carried out with the use of the determinant Quantum Monte Carlo.

[1] P. W. Anderson, in *Frontiers and Borderlines in Many-Particle Physics*, edited by R. A. Broglia and J. R. Schrieffer (North-Holland, Amsterdam, 1988), pp. 1–47.

[2] P. A. Lee, N. Nagaosa, and X.-G. Wen, Rev. Mod. Phys. **78**, 17 (2006).

[3] F. C. Zhang and T. M. Rice, Phys. Rev. B **37**, 3759 (1988).

[4] M. Ogata and H. Fukuyama, Rep. Prog. Phys. **71**, 036501 (2008).

[5] E. Dagotto, Rev. Mod. Phys. **66**, 763 (1994).

[6] D. J. Scalapino, Rev. Mod. Phys. **84**, 1383 (2012).

[7] N. M. Plakida, Physica C **531**, 39 (2016).

[8] B. Edegger, V. N. Muthukumar, and C. Gros, Adv. Phys. **56**, 927 (2007).

[9] D. Eichenberger and D. Baeriswyl, Phys. Rev. B **76**, 180504 (2007).

[10] M. Capone and G. Kotliar, Phys. Rev. B **74**, 054513 (2006).

[11] D. Sénéchal, P.-L. Lavertu, M.-A. Marois, and A.-M. S. Tremblay, Phys. Rev. Lett. **94**, 156404 (2005)..

[12] J. Spałek, M. Zegrodnik, and J. Kaczmarczyk, Phys. Rev. B **95**, 024506 (2017).

[13] M. Zegrodnik and J. Spałek, Phys. Rev. B **95**, 024507 (2017).

[14] M. Zegrodnik and J. Spałek, Phys. Rev. B **96**, 054511 (2017).

[15] M. Zegrodnik and J. Spałek, New J. Phys. **20**, 063015 (2018).

[16] M. Zegrodnik and J. Spałek, Phys. Rev. B **98**, 155144 (2018).

[17] M. Fidrysiak, M. Zegrodnik, and J. Spałek, J. Phys.: Condens. Matter **30**, 475602 (2018).

[18] G.-q. Zheng, Y. Kitaoka, K. Ishida, and K. Asayama, J. Phys. Soc. Jpn. **64**, 2524 (1995).

[19] D. Rybicki, M. Jurkutat, S. Reichardt, C. Kapusta, and J. Haase, Nat. Commun. **7**, 11413 (2016).

[20] C. Weber, C. Yee, K. Haule, and G. Kotliar, Europhys. Lett. **100**, 37001 (2012).

[21] W. Ruan, C. Hu, J. Zhao, P. Cai, Y. Peng, C. Ye, R. Yu, X. Li, Z. Hao, C. Jin, X. Zhou, Z.-Y. Weng, and Y. Wang, Sci. Bull. **61**, 1826 (2016).

[22] C. Weber, K. Haule, and G. Kotliar, Phys. Rev. B **78**, 134519 (2008).

[23] A. Go and A. J. Millis, Phys. Rev. Lett. **114**, 016402 (2015).

[24] T. Yanagisawa and M. Miyazaki, Europhys. Lett. **107**, 27004 (2014).

[25] Y. F. Kung, C.-C. Chen, Y. Wang, E. W. Huang, E. A. Nowadnick, B. Moritz, R. T. Scalettar, S. Johnston, and T. P. Devereaux, Phys. Rev. B **93**, 155166 (2016).

[26] T. Yanagisawa, S. Koike, and K. Yamaji, Phys. Rev. B **64**, 184509 (2001).

[27] S. Tamura and H. Yokoyama, Phys. Proc. **81**, 5 (2016).

[28] C. Weber, T. Giamarchi, and C. M. Varma, Phys. Rev. Lett. **112**, 117001 (2014).

[29] T. Yanagisawa, M. Miyazaki, and K. Yamaji, J. Phys. Soc. Jpn. **78**, 013706 (2009).

[30] M. S. Hybertsen, M. Schlüter, and N. E. Christensen, Phys. Rev. B **39**, 9028 (1989).

[31] A. K. McMahan, J. F. Annett, and R. M. Martin, Phys. Rev. B **42**, 6268 (1990).

[32] D. van der Marel, J. van Elp, G. A. Sawatzky, and D. Heitmann, Phys. Rev. B **37**, 5136 (1988).

[33] A. Fujimori, Phys. Rev. B **39**, 793 (1989).

[34] H. Eskes, L. H. Tjeng, and G. A. Sawatzky, Phys. Rev. B **41**, 288 (1990).

[35] M. Hirayama, Y. Yamaji, T. Misawa, and M. Imada, Phys. Rev. B **98**, 134501 (2018).

[36] J. Kaczmarczyk, J. Spałek, T. Schickling, and J. Bünemann, Phys. Rev. B **88**, 115127 (2013).

[37] J. Kaczmarczyk, J. Bünemann, and J. Spałek, New J. Phys. **16**, 073018 (2014).

[38] M. M. Wysokiński, J. Kaczmarczyk, and J. Spałek, Phys. Rev. B **94**, 024517 (2016).

[39] K. Münster and J. Bünemann, Phys. Rev. B **94**, 045135 (2016).

[40] J. Bünemann, T. Schickling, and F. Gebhard, Europhys. Lett. **98**, 27006 (2012).

[41] F. Gebhard, Phys. Rev. B **41**, 9452 (1990).

[42] M. Abram, M. Zegrodnik, and J. Spałek, J. Phys.: Condens. Matter **29**, 365602 (2017).

[43] Z.-X. Shen, D. S. Dessau, B. O. Wells, D. M. King, W. E. Spicer, A. J. Arko, D. Marshall, L. W. Lombardo, A. Kapitulnik, P. Dickinson, S. Doniach, J. DiCarlo, A. G. Loeser, and C. H. Park, Phys. Rev. Lett. **70**, 1553 (1993).

[44] W. N. Hardy, D. A. Bonn, D. C. Morgan, R. Liang, and K. Zhang, Phys. Rev. Lett. **70**, 3999 (1993).

[45] T. P. Devereaux and R. Hackl, Rev. Mod. Phys. **79**, 175 (2007).

[46] D. J. Van Harlingen, Rev. Mod. Phys. **67**, 515 (1995).

[47] F. Becca and S. Sorella, *Quantum Monte Carlo Approaches For Correlated Systems* (Cambbridge University Press, Cambridge, UK, 2017).

[48] W. M. C. Foulkes, L. Mitas, R. J. Needs, and G. Rajagopal, Rev. Mod. Phys. **73**, 33 (2001).

[49] A. Biborski and A. P. Kądzielawa, QMT: Quantum Metallization Tools Library, 2014, https://bitbucket.org/azja/qmt.

[50] A. Biborski, A. P. Kądzielawa, and J. Spałek, Phys. Rev. B **98**, 085112 (2018).

[51] N. P. Armitage, P. Fournier, and R. L. Greene, Rev. Mod. Phys. **82**, 2421 (2010).

[52] A. Avella, F. Mancini, F. P. Mancini, and E. Plekhanov, Eur. Phys. J. B **86**, 265 (2013).

[53] H. Ebrahimnejad, G. A. Sawatzky, and M. Berciu, Nat. Phys. **10**, 951 (2014).

[54] H. Ebrahimnejad, G. A. Sawatzky, and M. Berciu, J. Phys.: Condens. Matter **28**, 105603 (2016).

[55] E. Pavarini, I. Dasgupta, T. Saha-Dasgupta, O. Jepsen, and O. K. Andersen, Phys. Rev. Lett. **87**, 047003 (2001).

[56] B. Keimer, S. A. Kivelson, M. R. Norman, S. Uchida, and J. Zaanen, Nature (London) **518**, 179 (2015).

[57] L. Spanu, M. Lugas, F. Becca, and S. Sorella, Phys. Rev. B **77**, 024510 (2008).

[58] J. Kaczmarczyk and J. Spałek, Phys. Rev. B **84**, 125140 (2011).